NASA/TM–2015–218734

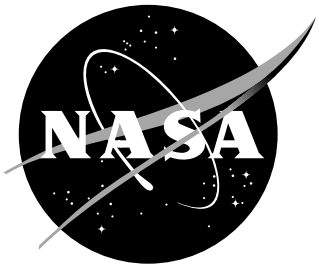

Minimum-Cost Aircraft Descent Trajectories with a Constrained Altitude Profile

Minghong G. Wu
Research Scientist, University of California, Santa Cruz, Moffett Field, California, 94035-1000

Alexander V. Sadovsky
Aerospace Engineer, NASA Ames Research Center, Moffett Field, California, 94035-1000

April 2015

NASA STI Program . . . in Profile

Since its founding, NASA has been dedicated to the advancement of aeronautics and space science. The NASA scientific and technical information (STI) program plays a key part in helping NASA maintain this important role.

The NASA STI Program operates under the auspices of the Agency Chief Information Officer. It collects, organizes, provides for archiving, and disseminates NASA's STI. The NASA STI Program provides access to the NASA Aeronautics and Space Database and its public interface, the NASA Technical Report Server, thus providing one of the largest collection of aeronautical and space science STI in the world. Results are published in both non-NASA channels and by NASA in the NASA STI Report Series, which includes the following report types:

- TECHNICAL PUBLICATION. Reports of completed research or a major significant phase of research that present the results of NASA programs and include extensive data or theoretical analysis. Includes compilations of significant scientific and technical data and information deemed to be of continuing reference value. NASA counterpart of peer-reviewed formal professional papers, but having less stringent limitations on manuscript length and extent of graphic presentations.
- TECHNICAL MEMORANDUM. Scientific and technical findings that are preliminary or of specialized interest, e.g., quick release reports, working papers, and bibliographies that contain minimal annotation. Does not contain extensive analysis.
- CONTRACTOR REPORT. Scientific and technical findings by NASA-sponsored contractors and grantees.
- CONFERENCE PUBLICATION. Collected papers from scientific and technical conferences, symposia, seminars, or other meetings sponsored or co-sponsored by NASA.
- SPECIAL PUBLICATION. Scientific, technical, or historical information from NASA programs, projects, and missions, often concerned with subjects having substantial public interest.
- TECHNICAL TRANSLATION. English-language translations of foreign scientific and technical material pertinent to NASA's mission.

Specialized services also include creating custom thesauri, building customized databases, and organizing and publishing research results.

For more information about the NASA STI Program, see the following:

- Access the NASA STI program home page at ***http://www.sti.nasa.gov***
- E-mail your question via the Internet to help@sti.nasa.gov
- Fax your question to the NASA STI Help Desk at 443-757-5803
- Phone the NASA STI Help Desk at 443-757-5802
- Write to:
  NASA STI Help Desk
  NASA Center for AeroSpace Information
  7115 Standard Drive
  Hanover, MD 21076–1320

NASA/TM–2015–218734

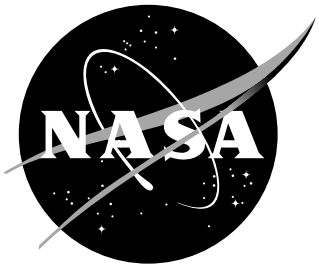

Minimum-Cost Aircraft Descent Trajectories with a Constrained Altitude Profile

Minghong G. Wu
Research Scientist, University of California, Santa Cruz, Moffett Field, California, 94035-1000

Alexander V. Sadovsky
Aerospace Engineer, NASA Ames Research Center, Moffett Field, California, 94035-1000

National Aeronautics and
Space Administration

Ames Research Center
Moffett Field, California, 94035-1000

April 2015

Available from:

NASA Center for AeroSpace Information
7115 Standard Drive
Hanover, MD 21076-1320
443-757-5802

Abstract

An analytical formula for solving the speed profile that accrues minimum cost during an aircraft descent with a constrained altitude profile is derived. The optimal speed profile first reaches a certain speed, called the minimum-cost speed, as quickly as possible using an appropriate extreme value of thrust. The speed profile then stays on the minimum-cost speed as long as possible, before switching to an extreme value of thrust for the rest of the descent. The formula is applied to an actual arrival route and its sensitivity to winds and airlines' business objectives is analyzed.

Nomenclature

A	Area on the xs-plane enclosed by a closed contour
C_D	Drag coefficient
C_L	Lift coefficient
C_{d0}	Zero-lift drag coefficient
D	Drag
$\overline{D}$	Effective drag per unit mass
F	$c_f\overline{D}$
H	Hamiltonian of the Problem
I	Integrand in the area integral on xs-space
$\tilde{I}$	$(V+w)^2 I$
J	Direct Operating Cost
K	Lift-induced drag coefficient
L	Aircraft's Lift
$M,\ P$	Functions of x and V
R	Local turn radius
S	Aircraft's wing Area
T	Thrust
$\overline{T}$	Thrust per unit mass
$\overline{T}_{\max}$	Maximum-thrust per unit mass
$\overline{T}_{\min}$	Minimum-thrust per unit mass
$\overline{T}_{\mathrm{mc}}$	Thrust per unit mass on the minimum-cost speed
V	Airspeed
$\dot{V}$	Airspeed change rate
V^i	Initial airspeed
V^f	Final airspeed
V_{mc}	Minimum-cost speed
W	Aircraft's weight
X^{fe}	Flat-Earth Coordinate along a constant latitude
Y^{fe}	Flat-Earth Coordinate along a constant longitude
c_f	Thrust-specific fuel consumption
g	Gravity of earth
h	Aircraft's altitude
$\dot{h}$	Aircraft's altitude rate

p_f	Fuel Price
r	Cost Index
$\overline{r}$	Cost Index per unit mass per unit fuel price
t	Time
w	Wind component along the route
x	Ground Path distance
$\dot{x}$	Path distance rate
x^i	Initial ground path distance
x^f	Final ground path distance
Γ	Trajectory on the xs-plane
α	Best-range speed modulating factor
γ_i	Inertial flight-path angle
γ_a	Aerodynamic flight-path angle
λ_s	Costate of s
λ_x	Costate of x
ρ	Air density

1 Introduction

Efficient arrival operations in the terminal airspace have been the focus of air traffic management research for years. In recent years, significant efforts have been made to integrate existing and new technologies as well as new procedures to manage arrival flights in a trajectory-based, precision-scheduling fashion [1, 2]. Arrival flights are scheduled based on specific arrival routes defined all the way from the top-of-descent to the runway threshold [3, 4]. With this trajectory-based, precision-scheduling approach, air traffic controllers use speed clearances to guide flights to meet the schedule and maintain separation while reserving vectoring clearances for exceptions only. This speed-centric approach is in contrast to the conventional approach, in which aircraft routinely follow air traffic controllers' vectoring clearances as soon as they enter the terminal airspace.

An arrival procedure that supports trajectory-based, precision-scheduling requires a flight to traverse a specific route consisting of a ordered sequence of *waypoints*[1]. Such a procedure also imposes altitude restrictions at certain waypoints. The altitude restrictions provide vertical separation for different traffic flows, keep specific arrival flows in the same controller's sector, and account for terrain constraints [6]. An altitude restriction can have an upper bound, a lower bound, or both. While the upper and lower bounds can be made different to accommodate aircraft types' varying performance envelopes in the en route airspace, ATC can rarely afford such flexibility in a congested terminal airspace with complex traffic flows. Therefore, altitude restrictions in the terminal airspace as well as some transition airspace always have identical upper and lower bounds. When such altitude restrictions are closely spaced, arrival flights are observed to fly a sequence of constant flight-path angle (FPA) segments.

While an arrival flight's altitude profile is much constrained by considerations related to

[1] A waypoint is a geographical position defined by its latitude and longitude coordinates [5].

traffic flow, terrain, and safety, its speed profile leaves room for optimization. Cost-effective speed strategies are of common interest to airlines and ATC, and insight of such can benefit both parties. Specifically, the insight can be used to improve scheduling efficiencies in the ground automation tools for ATC. For example, the Terminal Sequencing and Spacing (TSS) system in the United States requires route-specific nominal speed profiles as input parameters for computing the arrival flights' schedule. Each aircraft is scheduled by TSS's scheduler at route merge points such as the *meter fix*[2] and the runway threshold [1, 3]. Route-specific nominal speed profiles are used for ordering aircraft on the schedule. TSS then computes for each aircraft a speed profile that would meet the schedule, perturbing the speed profile from the nominal one to meet separation restrictions at the merge points if necessary [8]. While the nominal speed profiles are critical to the efficiency of the schedule, little attention has been paid to their selection. They have been selected only to ensure flyability without any check for systemic fuel or cost efficiency. This lack of consideration motivated the study in this work.

Trajectories that minimize fuel or cost have been studied extensively. A fairly comprehensive review of work in this area can be found in [9]. Early work considered optimization of trajectories in climb, cruise, and descent phases combined [10–13]. Such analysis can be formulated as a multi-phase optimization problem [14]. Some recent work analyzed descent only or cruise/descent trajectories [15–18] and investigated trade-off between fuel and flight time [19]. The optimal descent trajectory obtained from these work typically utilizes idle thrust engine control. However, none of these work considered altitude restrictions during the descent. Therefore, the optimal trajectory may violate the altitude restrictions in a trajectory-based arrival procedure and cannot be executed in operations without modification.

This paper derives the minimum-cost speed profile for an arrival flight following a specific route with a constrained altitude profile. The direct operating cost [20] serves as the objective functional to be minimized. The total engine thrust, referred to as thrust, is the control variable. The central result consists of an analytical formula for the speed profile. It reveals that an optimal speed profile generally gets to a minimum-cost speed as quickly as possible. It then stays on the minimum-cost speed as long as possible, until it has to leave to reach the final speed. The minimum-cost speed profile is computed for Boeing 737-800 along an actual route, and its sensitivity to wind and airlines' business objectives is investigated.

The rest of the paper is organized as follows: Section 2 gives additional background information and discusses the modeling assumptions; Section 3 formulates the optimal control model; Section 4 derives the analytical formula for the speed profile; Section 5 applies the formula to an actual arrival route and compares the minimum-cost trajectory to that of a simulated flight; Section 6 summarizes the findings and discusses the potential applications of the minimum-cost speed profile.

[2] A meter fix is a waypoint at the boundary of the terminal area that can have scheduled times of arrival for flights during high-density traffic [7].

2 Background

2.1 Minimum-Cost Descent

An arrival flight transitions from cruise to descent at a distance of 100 to 150 nmi from the destination airport. In the absence of wind and altitude restrictions, the most fuel-efficient operation for an arrival flight is to maintain at the *best-range speed* in cruise until the top-of-descent point for an idle-thrust descent at the aircraft's *minimum-drag speed* [20]. However, airlines can save time-related costs by flying an aircraft faster to the destination airport. If time saving is the sole objective, the ideal cruise and descent speeds would be the maximum speeds allowable by the aircraft performance envelope. In actual operations, airlines consider both fuel and time costs and the minimum-cost speeds lie between these two extremes. The relative importance of expediency to fuel is modeled by the Cost Index, a parameter selected by airlines during flight planning. The Cost Index varies from route to route and from aircraft type to aircraft type [21]. A zero Cost Index represents the case in which flight time does not contribute to the cost. A large Cost Index represents that expediency is more important than fuel.

2.2 Arrival Procedure

In the United States, arrival flights to major airports follow published arrival procedures called the Standard Terminal Arrival Route (STAR). While current STARs do not connect the route all the way to the runway threshold, they are expected to be extended to the runway in the near future to support trajectory-based operations [1]. For the rest of the paper, it is assumed that a specific route is defined for an arrival flight all the way to the runway threshold.

The aircraft descent trajectory considered in this work begins from the first altitude restriction along the arrival route and ends at the initial approach fix that is usually 5 to 10 nmi from the airport. The total path distance of the trajectory is between 50 and 100 nmi.

3 An Optimal Control Model for Aircraft Descent

3.1 Modeling Assumptions

The following assumptions are made throughout this section, grouped here by the different aspects of the operation.

1. Route geometry: The descent trajectory is modeled as a continuous curve in 3-dimensional airspace, parameterized by the ground path distance.
2. Aircraft kinematics and kinetics:
   (a) The aircraft is modeled as a point mass.
   (b) The weight of the aircraft is treated as a constant.

(c) The thrust acts along the direction of the flight path.

(d) Fuel flow is linear with thrust.

3. Flight conditions:

   (a) The wind velocity is constant in time. Crosswind and vertical wind are small compared to the airspeed and, therefore, is neglected.

   (b) Both the inertial and aerodynamic flight path angles are small enough that their cosines are assumed to equal 1.

3.2 Model Formulation

Let x denote the ground path distance of the aircraft's position along the coordinate defined by the horizontal path. By assumption (1), the altitude h of the aircraft, the air density ρ, and inertial flight path angle, γ_i, of the aircraft can each be represented as a function of x alone,

$$\begin{aligned} h &= h(x), \\ \rho &= \rho(x), \\ \tan\gamma_i &= \frac{dh}{dx}. \end{aligned} \tag{1}$$

The last equation is based on the sign convention that γ_i is negative for descent.

Let $V = V(t)$ denote the speed of the aircraft with respect to the air, i.e., the true airspeed. In the following sections, speed refers to the true airspeed unless noted otherwise. The wind along the route is denoted by

$$w = w(x) \tag{2}$$

and, by assumption (3a), is independent of time. By assumption (3b), the difference between the horizontal component of the true airspeed and the true airspeed itself is ignored:

$$\begin{aligned} V_{horiz} &\sim V \\ w_{horiz} &\sim w \end{aligned}$$

In the following state equations, T denotes thrust, D drag, γ_a the aerodynamic flight path angle, W the aircraft's weight, g the gravity of Earth, and the dot over a symbol denotes differentiation with respect to time:

$$\dot{x} = V + w, \tag{3a}$$

$$\dot{V} = g\left(\frac{T-D}{W} - \sin\gamma_a\right) - (V+w)\frac{dw}{dx}, \tag{3b}$$

where $D = D(x, V)$ and $x = x(t)$. The right-hand side of Eq. (3b) consists of forces from the thrust, drag, gravity, and the inertial force as a result of wind. Note the use of assumptions (2b) and (2c) in Eq. (3b). The FPAs γ_a and γ_i are related by

$$\dot{h} = V\sin\gamma_a = (V+w)\sin\gamma_i. \tag{4}$$

The use of γ_a in the state equations has been preferred to that of γ_i for brevity.

The aircraft's total engine thrust is bounded,

$$T_{\min} \leq T \leq T_{\max},$$

with the bounds determined by the engine's performance envelope.

The objective to be minimized is the direct operating cost, which is a sum of two terms corresponding to fuel and flight duration, respectively:

$$J = \int_0^{t^f} \left\{ \overbrace{p_f \times c_f \times [T(t) - T_{\min}] + f_0}^{\text{Fuel}} + \overbrace{p_f \times r}^{\text{Time}} \right\} dt. \tag{5}$$

Here, t^f stands for the arrival time at the end of the route, p_f the fuel price, c_f the thrust-specific fuel consumption, f_0 the minimum-thrust fuel rate, and r a constant Cost Index [20].

In what follows, it will be convenient to combine the drag, gravity, and wind gradient into the "effective drag per unit mass",

$$\overline{D} = \frac{g}{W}\left(D + W\sin\gamma_a\right) + (V + w)\frac{dw}{dx}, \tag{6}$$

and to normalize thrust to a "thrust per unit mass",

$$\overline{T} = \frac{g}{W}T. \tag{7}$$

These definitions simplify the state equations to

$$\dot{x} = V + w, \tag{8a}$$

$$\dot{V} = \overline{T} - \overline{D} \tag{8b}$$

The optimal control problem central to this paper is the problem with state variables x and V, control variable $\overline{T}$, state equations (8), initial time $t = 0$, final time t^f free, boundary conditions

$$\left.\begin{aligned} x(0) &= x^i, \\ V(0) &= V^i, \\ x(t^f) &= x^f, \\ V(t^f) &= V^f, \end{aligned}\right\} \tag{9}$$

control constraints

$$\overline{T}_{\min} \leq \overline{T} \leq \overline{T}_{\max}, \tag{10}$$

and the objective to minimize being the normalized cost per unit aircraft mass:

$$\overline{J} = \int_0^{t^f} \left(c_f\overline{T}(t) + \overline{r}\right) dt, \qquad \text{where } \overline{r} = \frac{g}{W}\left(-c_f T_{\min} + f_0 + r\right). \tag{11}$$

4 An Analytical Optimal Solution in Feedback Form

4.1 Comparison of Two Feasible State Trajectories

The optimal control problem (8), (9), (10), (11) has two state variables and one control variable which, furthermore, enters the state equations and the cost linearly. This special form of the problem allows one to find optimal control strategies using a technique based on Green's Theorem; see, e.g., [22]. This technique consists of comparing two feasible (i.e., compliant with (8), (9), (10), but possibly suboptimal) state trajectories for performance.

Let

$$\Gamma_1 = (x_1(t), V_1(t)),\ 0 \leq t \leq {t_1}^f,$$

and

$$\Gamma_2 = (x_2(t), V_2(t)),\ 0 \leq t \leq {t_2}^f,$$

be two feasible state trajectories corresponding to control strategies $\overline{T}_1(t)$ and $\overline{T}_2(t)$ with generally different final times. The respective operating costs (11) of the two trajectories can be briefly written

$$\overline{J_k} = \int_0^{t_k^f} \left[c_f \overline{T}_k(t) + \overline{r} \right]\ dt, \quad k = 1, 2.$$

The direct operating cost can be written as a path integral, along the state trajectory, of a differential form $P(x, V)\, dx + M(x, V)\, dV$ (derived explicitly in Appendix A), i.e.,

$$\overline{J_k} = \int_{\Gamma_k} \left[P(x,\, V)\, dx + M(x,\, V)\, dV \right], \quad k = 1, 2. \tag{12}$$

At constant airspeed, i.e. $dV = 0$, the quantity P has the interpretation of steady-state cost per unit ground path distance.

The difference

$$\overline{J_1} - \overline{J_2} \tag{13}$$

is the difference in performance between the two state trajectories. Henceforth, assume that the two trajectories share no other states besides $(x^i,\ V^i)$ and $(x^f,\ V^f)$. This assumption, which entails no loss of generality but simplifies analysis, implies that Γ_1 and reverse-oriented Γ_2 together constitute a *closed contour* [23], denoted here by $\Gamma_1 \cup -\Gamma_2$ and, for definiteness, assumed oriented counter-clockwise. See Figure 1 for a notional illustration. Expression (13) can be written as a path integral along the aforementioned closed contour:

$$\oint_{\Gamma_1 \cup -\Gamma_2} \left(P\, dx + M\, dV \right).$$

By Green's Theorem, the latter integral can be written as an integral over the area A enclosed and oriented by the contour:

$$\iint_A \left(\frac{\partial M}{\partial x} - \frac{\partial P}{\partial V} \right)\, dx\, dV. \tag{14}$$

The two state trajectories can now be compared for performance by using the knowledge

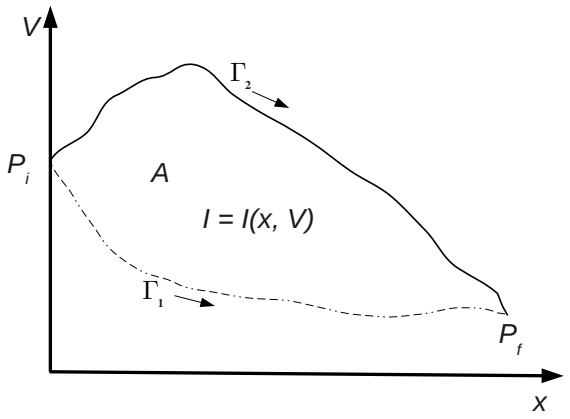

Figure 1. Green's Theorem predicts $J_1 < J_2$ if $I < 0$ everywhere in the enclosed area; and $J_1 > J_2$ if $I > 0$ everywhere in the enclosed area.

of the integrand

$$I \equiv \frac{\partial M}{\partial x} - \frac{\partial P}{\partial V}$$

to examine the sign of the difference (13). In particular, if I is nonnegative in and on the boundary of A, then Γ_2 performs as well as does Γ_1 or better. Consequently, a comparison of two feasible state trajectories reduces to an examination of the sign of I in the appropriate regions of the state space. This examination will now be carried out.

By the derivation in Appendix A,

$$P = \frac{c_f \overline{D} + \overline{r}}{V + w},\ M = c_f, \tag{15}$$

and, consequently,

$$I = \frac{\partial c_f}{\partial x} - \frac{\partial}{\partial V}\left(\frac{c_f \overline{D} + \overline{r}}{V + w}\right).$$

For typical commercial aircraft and descent FPAs, c_f does not vary substantially with the ground path distance. Therefore, the first term on the right hand side can be ignored without noticeable effects on the results, i.e.,

$$I \simeq -\frac{\partial}{\partial V}\left(\frac{c_f \overline{D} + \overline{r}}{V + w}\right). \tag{16}$$

For aircraft with typical drag formulas (described in detail below) and, within the range of airspeeds considered, one finds that the zero-level set $[I = 0]$ is the graph of a function $V_{\rm mc}(x)$ called the minimum-cost speed. The subscript mc stands for minimum cost because

$$\left.\frac{\partial P}{\partial V}\right|_{V=V_{\rm mc}} = 0$$

and

$$\frac{\partial^2 P}{\partial V^2} > 0, \tag{17}$$

which will be shown at the end of this section. It follows that

$$I(x,V) \begin{cases} < 0 & \text{if } V > V_{\text{mc}}(x), \\ = 0 & \text{if } V = V_{\text{mc}}(x), \\ > 0 & \text{if } V < V_{\text{mc}}(x). \end{cases} \tag{18}$$

To conclude the section, we justify stipulation (17). A typical drag polar [24] for modeling drag is

$$D = \frac{1}{2}\rho V^2 S C_D = \frac{1}{2}\rho V^2 S \left(C_{d0} + K {C_L}^2\right),$$

where C_L denotes the lift coefficient, C_D the drag coefficient, C_{d0} the zero-lift drag coefficient, K the lift drag constant, S the aircraft's wing area, and $\rho = \rho(x)$ the air density. Replacing C_L with its definition [24],

$$L = W\sqrt{1 + \frac{V^4}{g^2 R^2}} = \frac{1}{2}\rho V^2 S C_L,$$

where R is the instantaneous turn radius, the drag can be written

$$D = \frac{1}{2}\rho V^2 S C_{d0} + \frac{K W^2}{\frac{1}{2}\rho V^2 S}\left(1 + \frac{V^4}{g^2 R^2}\right). \tag{19}$$

Equations (6), (16), (19) and the dependency of D on V together imply that

$$I \sim \begin{cases} -\dfrac{g}{2W}\rho S C_{d0} - \dfrac{2KW}{\rho S g R^2} < 0, \text{ for a large } V, \\ \dfrac{6KW}{g\rho S V^4} > 0, \text{ for a small } V. \end{cases} \tag{20}$$

It can also be shown that

$$\frac{\partial^2 P}{\partial V^2} = -\frac{\partial I}{\partial V} = \frac{24KW}{g\rho V^5 S} > 0, \text{ if } w = \overline{r} = 0. \tag{21}$$

Results (20) and (21) together imply (18).

Numerical evidence obtained for the case when w and $\overline{r}$ have realistic nonzero values suggests that the inequality in Eq. (21) always holds for the range of V considered, hence confirming (17) and (18).

4.2 Optimal State Trajectories and Control Strategies

The following observation will be instrumental throughout this section: *the curve in the state space traversed by a feasible state trajectory* $(x(t), V(t))$ *can be parameterized by* x

instead of by t; i.e., can be viewed as the graph of a function $V = V(x)$. This follows from the fact that, by dividing Eq. (8b) by Eq. (8a), one obtains

$$\frac{dV}{dx} = \frac{\overline{T} - \overline{D}}{V + w} \text{ is finite.}$$

Therefore, in what follows, whenever convenient, a state trajectory $(x(t), V(t))$ will be treated as a function $V = V(x)$ without further explanation.

The following lemma is a direct consequence of the results of Section 4.1. The five parts of the lemma are illustrated, respectively, by the five panels of Figure 2. It will be convenient to use the control-theoretic terms of *admissibility* [25] and *attainability*: A control value $\overline{T}$ satisfying (10) is said to be admissible. This term will be applied as well to a control strategy with the value $\overline{T}(t)$ admissible at every t. A state trajectory corresponding to an admissible control strategy will be referred to as attainable. The last part of the following lemma addresses the situation when not all segments of $[I = 0]$ are attainable trajectories.

Lemma 1 *Consider an initial state* $\mathbf{a} = (x_a, V_a)$ *and a final state* $\mathbf{b} = (x_b, V_b)$*, with* $x_a < x_b$*. For (a) through (d), consider two attainable state trajectories* $(x_1(t), V_1(t))$ *and* $(x_2(t), V_2(t))$ *that have the same initial state* $\mathbf{a}$ *and the same final state* $\mathbf{b}$*:*

(a) If $\mathbf{a}$ *is above* $[I = 0]$*,* $\mathbf{b}$ *is on* $[I = 0]$*, and*

$$V_{mc}(x) \le V_1(x) \le V_2(x) \quad \text{for } x_a \le x \le x_b,$$

then $V_1(x)$ *outperforms* $V_2(x)$*.* (This is because the integrand I in the area A enclosed by $\Gamma_1 \cup -\Gamma_2$ is negative.)

(b) If $\mathbf{a}$ *is below* $[I = 0]$*,* $\mathbf{b}$ *is on* $[I = 0]$*, and*

$$V_2(x) \le V_1(x) \le V_{mc}(x) \quad \text{for } x_a \le x \le x_b,$$

then $V_1(x)$ *outperforms* $V_2(x)$*.*

(c) If $\mathbf{a}$ *is on* $[I = 0]$*,* $\mathbf{b}$ *is above* $[I = 0]$*, and*

$$V_{mc}(x) \le V_1(x) \le V_2(x) \quad \text{for } x_a \le x \le x_b,$$

then $V_1(x)$ *outperforms* $V_2(x)$*.*

(d) If $\mathbf{a}$ *is on* $[I = 0]$*,* $\mathbf{b}$ *is below* $[I = 0]$*, and*

$$V_2(x) \le V_1(x) \le V_{mc}(x) \quad \text{for } x_a \le x \le x_b,$$

then $V_1(x)$ *outperforms* $V_2(x)$*.*

(e) Suppose $\mathbf{a}$ *and* $\mathbf{b}$ *are on the curve* $[I = 0]$*, and let* $\mathbf{ab}$ *denote the segment of* $[I = 0]$ *connecting these two states. If a segment* $\mathbf{a'b'}$ *of* $[I = 0]$ *is contained in* $\mathbf{ab}$ *and is not an attainable state trajectory (i.e., state* $\mathbf{b'}$ *cannot be reached from* $\mathbf{a'}$ *using admissible controls), then the optimal state trajectory from* $\mathbf{a}$ *to* $\mathbf{b}$ *consists of three segments: the segment of* $[I = 0]$ *from* $\mathbf{a}$ *to a state* $\mathbf{a}_1$ *on* $\mathbf{aa'}$*, one (attained by a suitable extreme value of control) from* $\mathbf{a}_1$ *to a state* $\mathbf{b}_1$ *on* $\mathbf{b'b}$*, and the segment of* $[I = 0]$ *from* $\mathbf{b}_1$ *to* $\mathbf{b}$*.*

The optimal trajectory described in the last part, (e), of the Lemma is completely determined by the point of intersection (the gray dot in Fig. 2(e)) between $\mathbf{a}'\mathbf{b}'$ and trajectory $\mathbf{a}_1\mathbf{b}_1$; i.e., by the choice of that state on $\mathbf{a}'\mathbf{b}'$ which minimizes the cost of getting from $\mathbf{a}$ to $\mathbf{b}$. Since segment $\mathbf{a}'\mathbf{b}'$ is closed and bounded, such a state necessarily exists.

In summary, the optimal trajectory goes towards $[I = 0]$ as rapidly as possible, as in Figure 2(a) and 2(b), and leaves $[I = 0]$ as late as possible, as in Figure 2(c) and 2(d). This observation along with Eq. (8b) suggests that extreme values of $\overline{T}$ must be used in getting the optimal trajectory to or from $[I = 0]$. That the optimal trajectory must, in fact, use $\overline{T}_{\min}$ or $\overline{T}_{\max}$ when it is not on the $[I = 0]$ curve, can be proved using the *Hamiltonian* [26] of the problem,

$$H = c_f\overline{T} + \overline{c_i} + \lambda_x(V + w) + \lambda_s\left(\overline{T} - \overline{D}\right), \tag{22}$$

where λ_x and λ_s are the respective costate variables of x and V. The optimal control minimizes (per the sign convention in [26]) the Hamiltonian at every point of the trajectory. The Hamiltonian H is linear in $\overline{T}$ and is minimized by:

$$\overline{T} = \begin{cases} \overline{T}_{\min} & \text{if } \frac{\partial H}{\partial \overline{T}} > 0 \\ \overline{T}_{\max} & \text{if } \frac{\partial H}{\partial \overline{T}} < 0. \end{cases} \tag{23}$$

If $\partial H/\partial\overline{T} = 0$, then the optimal control is on a *singular arc* [26]. The curve $[I = 0]$ turns out to be the singular arc of the Hamiltonian. In particular, for an optimal trajectory passing through a state in $I < 0$ and later intersecting $[I = 0]$, as in Lemma 1(a), the optimal control at that state is $\overline{T}_{\min}$. Similarly, for a state on an optimal trajectory passing through a state in $I > 0$ and later intersecting $[I = 0]$, as in Lemma 1(b), the optimal control at that state is $\overline{T}_{\max}$.

This classification of optimal control strategies can also be carried out by more elementary means, without involving the Hamiltonian formalism, but expending more verbiage. This simpler approach to optimal control classification is presented in Appendix B.

4.3 Control on the Minimum-Cost Speed Curve

The control that keeps the aircraft on the minimum-cost speed curve, $\overline{T}_{\text{mc}}$, is computed here by setting the right-hand side of Eq. (16) to zero and using the state equations (8). For convenience, define

$$\tilde{I} \equiv (V + w)^2 I. \tag{24}$$

Since $(V + w)$ is never zero in the range of airspeed and wind considered, the curves $[I = 0]$ and $[\tilde{I} = 0]$ coincide.

The following equality holds on $[\tilde{I} = 0]$:

$$\left.\frac{d\,V}{d\,x}\right|_{\tilde{I}=0} = -\left(\frac{\partial \tilde{I}}{\partial V}\right)^{-1}\frac{\partial \tilde{I}}{\partial x}. \tag{25}$$

Defining

$$F \equiv c_f\overline{D},$$

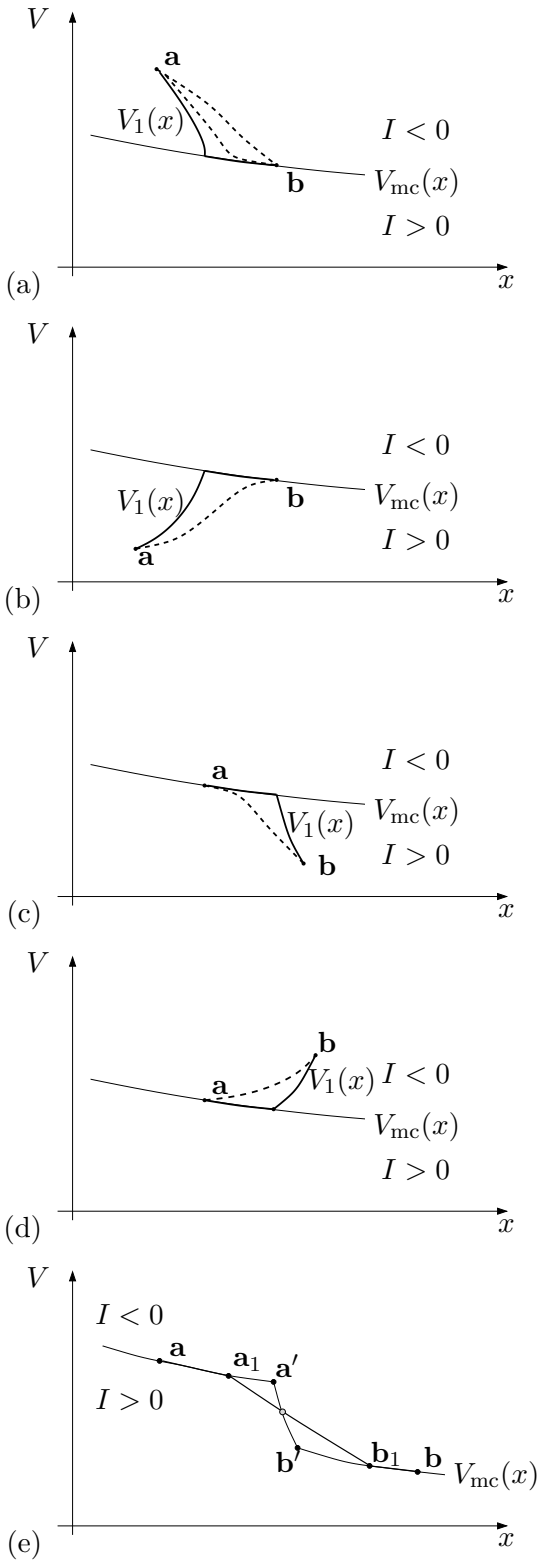

Figure 2. A notional illustration of Lemma 1. In panels (a) through (d), the trajectories from state **a** to state **b** shown in solid outperform those shown dashed.

and substituting Eqs. (24) and (16) into the right-hand side of Eq. (25), one obtains

$$\left.\frac{d\,V}{d\,x}\right|_{\tilde{I}=0} = \left[(V+w)\frac{\partial^2 F}{\partial V^2}\right]^{-1}\left[-\frac{\partial F}{\partial V}\frac{dw}{dx}+\frac{\partial F}{\partial x}-(V+w)\frac{\partial^2 F}{\partial x\,\partial V}\right], \tag{26}$$

From Eqs. (8) and (26), one obtains

$$\overline{T}_{\mathrm{mc}} = \overline{D} + \left(\frac{\partial^2 F}{\partial V^2}\right)^{-1}\left[-\frac{\partial F}{\partial V}\frac{dw}{dx}+\frac{\partial F}{\partial x}-(V+w)\frac{\partial^2 F}{\partial x\,\partial V}\right]. \tag{27}$$

With analytic expressions for the drag and the wind, the right-hand side of Eq. (27) can be evaluated for specific values of x and V. The thrust T_{mc} on $[I=0]$ is given by

$$T_{\mathrm{mc}} = \frac{W}{g}\overline{T}_{\mathrm{mc}}.$$

The thrust $\overline{T}_{\mathrm{mc}}$ computed using Eq. (27) can turn out to violate the admissibility condition (10) on an interval of the x-axis, leading to the situation of Lemma 1(e). In this case, the optimal trajectory leaves the minimum-cost speed curve with an extremal value of thrust until it either rejoins the minimum-cost speed curve or reaches the final state.

4.4 $V_{\mathbf{mc}}$ with Constant c_f and without Wind

The content of this section is a number of consequences derived from the above results for the special case when c_f is assumed constant, and wind speed assumed is zero at all altitudes. Under the assumption of constant c_f, Eq. (24) simplifies to

$$\tilde{I} = -(V+w)^2 c_f \frac{\partial}{\partial V}\left(\frac{\overline{D}+\overline{r}/c_f}{V+w}\right) = 0. \tag{28}$$

Furthermore, if the wind effect is negligible, then

$$\tilde{I} = -V^2 c_f \frac{\partial}{\partial V}\left(\frac{\overline{D}+\overline{r}/c_f}{V}\right) = 0. \tag{29}$$

By using Eqs. (6) and (19) to model the drag, Eq. (29) is solved analytically for V. The minimum-cost speed is found to be

$$V_{\mathrm{mc}}(x)^2 = \frac{(W/S)}{C_{d0}\,\rho(x)}\left[\alpha+\sqrt{\alpha^2+12KC_{d0}}\right]. \tag{30}$$

Here

$$\alpha = \sin\gamma_i + \frac{\overline{r}}{c_f g}$$

captures the combined effect of the FPA and of the Cost Index on the minimum-cost speed, In particular, α increases with $\overline{r}$ and with γ_i in a neighborhood of $\gamma_i = 0$.

Equality (30) has the following interpretations and implications

* The minimum-cost speed V_{mc} can be regarded as a modified *best-range speed* modulated by the factor α. For a flight segment which is level (i.e., with FPA zero) and has a zero Cost Index, the resulting special case $\alpha = 0$ corresponds to an V_{mc} equal to the best-range speed at an altitude specified by $h(x)$ [24].

* The minimum-cost speed $V_{\text{mc}}(x)$ decreases with altitude due to air density change.

* The minimum-cost speed $V_{\text{mc}}(x)$ increases with α, which means V_{mc} increases with γ_i and with the Cost Index.

5 Case Study: GEELA Arrival Route to the Phoenix Airport

5.1 Route Definition and Test Conditions

This section investigates the sensitivity of the optimal speed profile to the wind condition and Cost Index, explores the effects of certain modeling assumptions on the fuel computation, and compares the computed optimal trajectory to a simulated flight trajectory. The specific example of an arrival procedure used as a basis for this section is a portion of the GEELA route from waypoint HYDRR to waypoint PHX08 (runway 8) of the Phoenix Airport.[3]

Figure 3 shows the waypoints and altitude restrictions specified in this procedure. The coordinates X^{fe} and Y^{fe} in Fig. 3 increase Eastward and Northward, respectively. Note that the origin of the coordinates is arbitrary, since this figure is mainly for demonstrating the scale of an arrival route. This procedure is closely based on current operations but has additional waypoints to precisely guide the arrival flights all the way to the runway. This procedure has been used in simulations conducted to test arrival management technologies [3]. The ground path distance of the entire route was constructed by connecting consecutive waypoints' positions and span roughly 54 nmi. The coordinate x, representing the ground path distance, starts negative and increases to 0 at the runway threshold. Turns were modeled as having a five nautical mile turn radius each. This approximate treatment of the turns decoupled the horizontal path from the speed. Lift was treated approximately as being equal to the aircraft weight all the time. These approximations have been used by trajectory generators of the ground automation systems [27].

Figure 4 shows the modeled altitude $h(x)$ of the GEELA route. The FPA is modeled as a constant on each segment between two consecutive waypoints, except varying near the waypoint so as to remain continuous. This change of FPA takes place after the aircraft has crossed the waypoint. A fixed change rate of $\pm 1^\circ$ per nmi was used to model these transient segments.

The air density was a function of the altitude computed from the standard atmosphere model. It was 0.778 kg^3/m at the beginning of the descent and 1.187 kg^3/m at the end.

The initial airspeed at the waypoint HYDRR, V^i, for the aircraft was chosen to be the calibrated airspeed (CAS) [24] of 260 knots (174.7 m/sec), required at HYDRR by the

[3]The GEELA route has two upstream branches that merge at HYDRR. Only the portion from HYDRR to the airport is analyzed in this work.

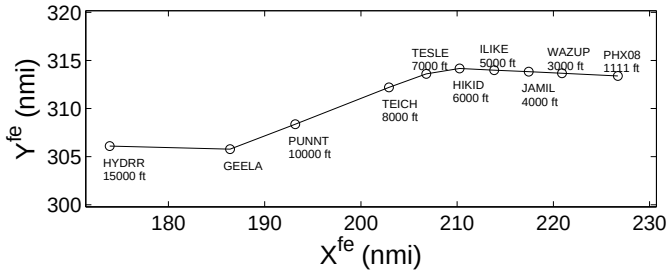

Figure 3. The GEELA arrival route to the Phoenix Airport.

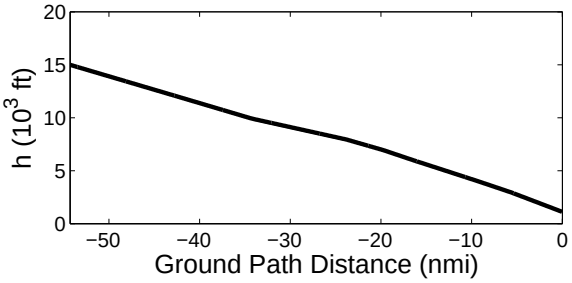

Figure 4. The altitude profile along the GEELA arrival route.

arrival procedure. The final speed at the runway PHX08, V^f, was set to a typical landing speed of 135 knots CAS (69.4 m/sec).

Boeing 737-800 aircraft type was modeled using the Base of Aircraft Database (BADA) 3.8 [28]. Flap schedule was not considered and only the clean configuration was used. The minimum-cost speed curve, $V_{\rm mc}(x)$ (see Fig. 2), was computed using Eq. (28) for the entire range of x. Substituting Eq. (19) into Eq. (28), a 5th-order polynomial in V was obtained whose coefficients depended on x. The polynomial reduces to 4th order when $w = 0$, in which case $V_{\rm mc}$ can be computed from Eq. (30). In all test conditions, one and only one real root between V^i and V^f was found for each x.

The optimal control strategy were applied to four benchmark conditions, labeled as Min-Fuel, Headwind, Tailwind, and Fuel-and-Time. These conditions differ only in the choice of wind function and Cost Index, listed in Table 1 and justified in the following sections.

Table 1. Parameters that define the four benchmark conditions.

Condition	Wind Gradient (see Eq. (2)) $w(x)$ (knots; x in nmi)	Cost Index (see Eq. (5)) r (\$/hr / (cents / lb))
Min-Fuel	0	0
Headwind	$-3.79 + 0.226x$	0
Tailwind	$1.03 - 0.301x$	0
Fuel-and-Time	0	30

Table 2. Flight times and fuel burn for the four conditions.

Condition	Flight Time (sec)	Fuel Burn (lb)
Min-Fuel	846	127
Headwind	830	166
Tailwind	854	82
Fuel-and-Time	801	150

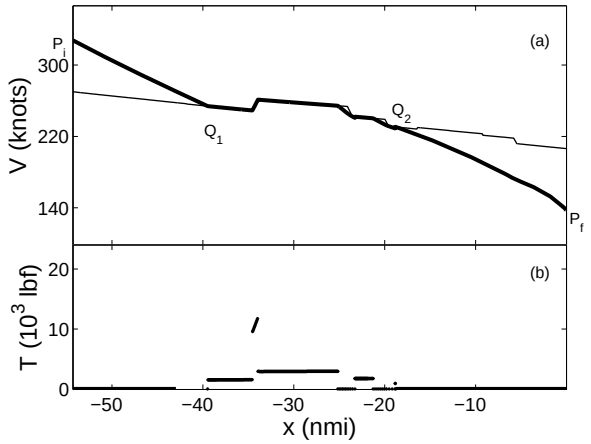

Figure 5. The minimum-cost speed profile and control strategy for the Min-Fuel condition.

In all conditions, the initial airspeed is above the minimum-cost speed and the final airspeed is below the minimum-cost speed, corresponding to Lemma 1(a) and 1(c), respectively. The discussion in Section 4.2 indicates that an extreme value of thrust, $\overline{T}_{\min}$, must be used in the initial and final phases of the state trajectory. The speeds for those phases were found by integrating the state equations with that value of thrust forward from the first two boundary conditions of (9) and backward from the last two boundary conditions of (9). The integration was carried out numerically using MATLAB's [29] ode45 function. The thrust $\overline{T}_{\rm mc}$ was computed as a function of x using Eq. (27).

Table 2 summarizes the flight times and fuel burn obtained for the four conditions. Details of the control strategy and speed profile will be discussed for each condition in the following sections.

5.2 Min-Fuel Condition: No Wind, No Time Cost

Figure 5(a) shows the optimal speed profile. The thin line represents the minimum-cost speed, $V_{\rm mc}$. Q_1 and Q_2 stand for points that join a $T_{\min}$ speed profile with a $T_{\rm mc}$ speed profile. The value $V_{\rm mc}$ was computed essentially from Eq. (30). The rapid changes of $V_{\rm mc}$ at some values of x were due to change of the FPA before and after a waypoint. The general trend was that $V_{\rm mc}$ increased with increasing (shallower) γ_i. For example, the increase of $V_{\rm mc}$ near $x = -34$ nmi corresponded to the waypoint of PUNNT. Between PUNNT and TEICH, the FPA was shallower than before PUNNT (see Fig. 4), resulting in higher values of $V_{\rm mc}$.

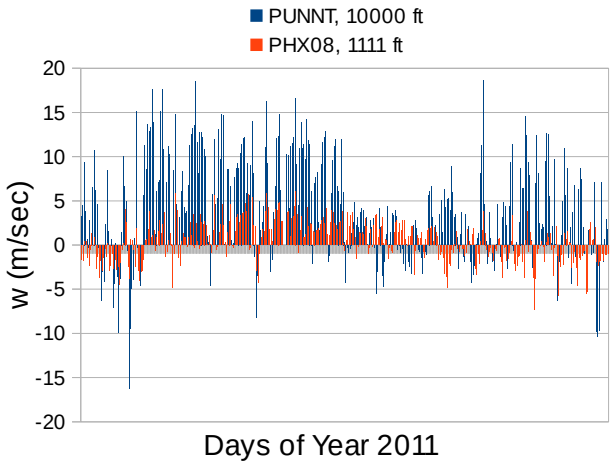

Figure 6. Daily averages of the along-the-route wind components at PUNNT and PHX08.

Figure 5(b) shows T as a function of x, which has non-zero thrust during the period of time when the trajectory follows the minimum-cost speed curve. The thrust for this period of time was equal to $T_{\rm mc}$. Shallower FPAs result in higher values of $T_{\rm mc}$ (e.g., on the segment from PUNNT to TEICH;). This corresponds to the physical intuition that a shallower descent does not convert as much potential energy to kinetic energy to compensate for the drag and therefore must use more thrust instead.

The speed profile shown in Fig. 5 turns out to be unattainable near $x = -24$ nmi and near $x = -20$ nmi. This situation corresponds to Lemma 1(e). In physical flight control, the effect of negative thrust could have been attained by using speed brakes. This use, however, would not result in the reduction of cost (11) as would negative thrust. In this model, the trajectory segment is computed, following the notation in Lemma 1(e), by iterating through possible segments of $\mathbf{a}_1\mathbf{b}_1$ until the minimum cost between $\mathbf{ab}$ is obtained. As expected, the actual optimal speed has a flatter $|dV/dx|$ than that of $|dV_{\rm mc}/dx|$ on these segments.

5.3 Headwind and Tailwind Conditions

The main purpose of studying these two wind conditions is to understand the effect of wind variation on the optimal control strategy and the resulting speed profile. To select representative winds conditions, winds along the GEELA route were computed using the two-hour look-ahead time, 40-km Rapid Update Cycle weather forecast [30] for year 2011. Twenty-four forecast winds were generated for each day on an hourly basis. Daily averages were computed for every day of year 2011 at the waypoints PUNNT and PHX08, two of the waypoints on the GEELA route (see Fig. 3).

Figure 6 shows the daily averages of the along-the-route components of wind at PUNNT and PHX08. The wind components for PUNNT and PHX08 were computed at 10,000 ft and 1,111 ft, respectively. The data indicated predominantly tailwinds for PUNNT all year long. Wind components at PHX08 were smaller in magnitude and varied somewhat by the season.

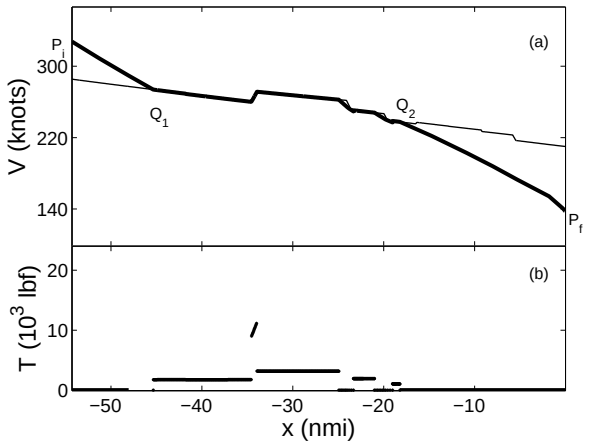

Figure 7. The speed profile and control strategy for the Headwind condition.

The Headwind and Tailwind conditions were selected from the two days of year 2011 that had the most negative and positive wind gradients, dw/dx, respectively. The Headwind condition was defined based on February 3's average wind, which had the most negative wind gradient. Both PUNNT and PHX08 experienced headwinds along the route on February 3. The Tailwind condition was defined based on February 19's average wind, which had the most positive wind gradient. Both PUNNT and PHX08 experienced tailwinds along the route on February 19. The wind gradient was assumed to be constant throughout the path, and was computed by dividing the difference of the wind components at PHX08 and PUNNT by the ground path distance between these two waypoints. The resulting wind functions are listed in Table 1.

The optimal speed profile and control strategy for the Headwind condition are shown in Fig. 7. The wind perturbed the minimum-cost speed curve noticeably, increasing V_{mc} by 16 knots at the beginning (x_i) of the trajectory and by only 4 knots at the end of the trajectory. The initial and final arcs descended faster in speed (more negative dV_{mc}/dx), causing the aircraft to stay longer on the minimum-cost speed curve than in the Min-Fuel condition. The thrust on the minimum-cost speed curve increased slightly when compared to the Min-Fuel condition. For transient segments on which the FPA increases rapidly around $x = -34$ nmi, the thrust takes relatively high values.

The optimal speed profile for the Tailwind condition is shown in Fig. 8(a). The wind perturbed the minimum-cost speed curve in the opposition direction, decreasing V_{mc} by 15 knots of V_{mc} at the beginning of the trajectory and by only 1 knot at the end of the trajectory. Fig. 8(b) shows the $T_{\min}$ arcs descended slower in speed, causing the aircraft to stay only a short distance on the minimum-cost speed curve. The thrust on the minimum-cost speed curve decreased slightly compared to the Min-Fuel condition.

The effect of wind on the minimum-cost speed is consistent with the dependency of the best-range speed on winds [24]: higher for headwind and lower for tailwind. Comparing the fuel burn to the Min-Fuel condition, the trajectory for the Headwind condition burns 36 lb more fuel while the trajectory for the Tailwind condition burns 31 lb less fuel (see Table 2).

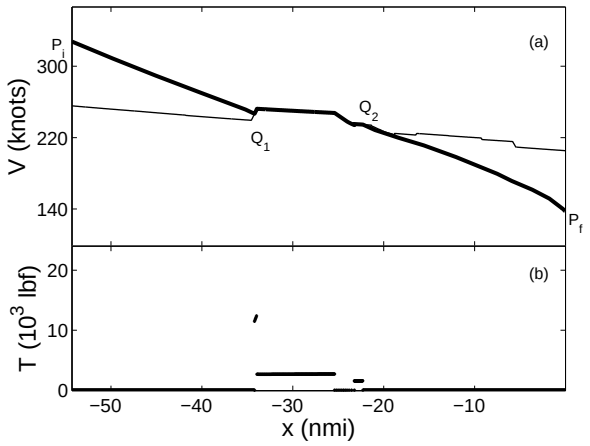

Figure 8. The speed profile and control strategy for the Tailwind condition.

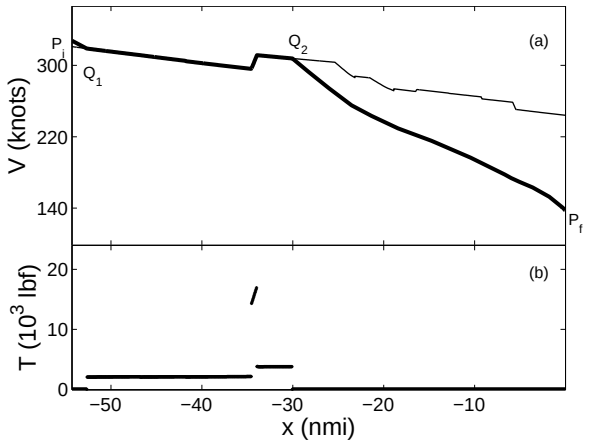

Figure 9. The minimum-cost speed curve and control strategy for the Fuel-and-Time Condition.

5.4 Fuel-and-Time Condition

The Fuel-and-Time condition considered both fuel and time costs. The Cost Index selected by airlines varies greatly from route to route and among aircraft types [20]. For B737, a typical value [20, 31] of

$$r = 30 \left(\frac{\$/\text{hr}}{\text{cents}\,\$/\text{lb}} \right)$$

was used for the analysis. The fuel price, p_f, was chosen to be 0.43 (\$/lb).

The optimal speed profile for the Fuel-and-Time condition is shown in Fig. 9(a). Compared to the Min-Fuel condition, the minimum-cost speed curve moves toward higher speeds significantly. This is because the aircraft must fly faster in order to reduce the time cost at the expense of the fuel cost. The minimum-cost speed curve was reached here much earlier than in the Min-Fuel condition. The speed profile for the Fuel-and-Time condition saved 45 seconds compared to that for the Min-Fuel condition (see Table 2), at the cost of 23 lb of fuel. Fig. 9(b) shows the required thrust T as a function of x. A large value of

thrust was required to accelerate the aircraft around $x = -34$ nmi due to the increase of the minimum-cost speed.

6 Conclusions

The key contribution of this paper is an exact feedback-control formula for the speed strategy that accrue minimum cost during a descent under altitude restrictions. The sensitivity of the optimal speed strategy to winds and airlines' business objectives was analyzed by applying the formula to an actual arrival route.

This analytical formula has the following potential applications:

Evaluation of arrival procedures: While most altitude restrictions are set by terrain, noise, and separation of traffic flows, speed restrictions can be compared to the minimum-cost speed profile to see whether the procedure can be refined to reduce aircrafts' direct operational costs. Since weather, airlines' business objectives, and aircraft types all affect the minimum-cost speed profile, a static arrival procedure should at best achieve systemic fuel/cost savings on an aggregated basis.

Scheduling efficiency of ground automation tools: Ground automation tools that assist ATC in scheduling arrival aircraft can take advantage of the minimum-cost speed profile and use this information to improve its scheduling efficiency. Specifically, the TSS system in the United States can use this information to improve the nominal speed profiles used as reference points for scheduling aircraft.

Guidance of small jets: While large commercial jets equipped with performance-based Flight Management Systems (FMS) have similar capabilities of computing company-preferred speed profile based on the airlines' business objective, aircraft performance model, and limited wind information, small jets such as regional and business jets are equipped with simpler FMS that cannot compute minimum-cost speed profiles. These jets accounts for 25% to 30% of the operations in the United States [32]. The methodology developed in this paper can be used to aid the airlines in the selection of speed profiles for these jets. The selection can presumably be made during the flight-planning phase.

A reference point for multi-aircraft operations: During periods of medium to heavy traffic, separation constraints must be taken into account and minimum-cost speed profiles may not be always feasible for individual aircraft. Nonetheless, the minimum-cost speed profiles can still be used as a reference point for evaluating the level of optimality of the system and for computing systemic cost-effective strategies.

Among the directions for future research, the following seem reasonable:

* Compare the minimum-cost speed profile to actual trajectories and determine how far-off is the current-day operations from optimality.

* Predict a systemic minimum-cost speed profile for a group of aircraft and a period of future time, using airlines' flight schedules and weather forecast.

* Accommodate hard-coded speed restrictions from ATC in the model formulation such as the 250 knots-or-below rule.

* Develop ways of applying the results herein to minimize the operating cost of multiple arrival flights in the terminal area. One key difficulty is the imposition of the separation constraint: every pair of aircraft must be separated by a minimum distance imposed by the FAA.

* Implement a generic solver for the minimum-cost speed in an extensible way such that it can work with various aircraft performance models.

References

1. Swenson, H.; Robinson III, J. E.; et al.: NASAs ATM Technology Demonstration–1: Moving NextGen Arrival Concepts from the Laboratory to the Operational NAS. *Journal of Air Traffic Control*, vol. 55, no. 2, 2013.

2. Hasevoets, N.; and Conroy, P.: AMAN Status Review 2010. *Eurocontrol, Edition number 0.1*, vol. 17, 2010.

3. Thipphavong, J.; Martin, L.; Swenson, H.; Lin, P.; and Nguyen, J.: Evaluation of the Terminal Area Precision Scheduling and Spacing System for near-term NAS application. *4th International Conference on Applied Human Factors and Ergonomics (AHFE)*, 2012.

4. *United States Standard for Required Navigation Performance (RNP) Approach Procedures with Special Aircraft and Aircrew Authorization Required (SAAAR)*. Order 8260.52, Federal Aviation Administration (FAA), June 2005.

5. Isaacson, D. R.; Sadovsky, A. V.; and Davis, D.: Tactical Scheduling for Precision Air Traffic Operations: Past Research and Current Problems. *Journal of Aerospace Information Systems*, vol. 11, 2014, pp. 234–257.

6. McElhatton, J.; Drew, C.; and Buchanan, P.: Crossing-Restriction Altitude Deviations on SIDs and STARs. *NASA ASRS Directline*, vol. 10, dec 1998, pp. 10–15.

7. Mulfinger, D.; and Sadovsky, A.: Design and Evaluation of a Stochastic Time-Based Arrival Scheduling Simulation System. *11th AIAA Aviation Technology, Integration, and Operations (ATIO) Conference*, AIAA-2011-6874, 2011.

8. Wong, G. L.: *The Dynamic Planner: the Sequencer, Scheduler, and Runway Allocator for Air Traffic Control Automation*. NASA/TM-2000-209586, 2000.

9. Franco, A.; and Rivas, D.: Analysis of Optimal Aircraft Cruise with Fixed Arrival Time Including Wind Effects. *Aerospace Science and Technology*, vol. 32, no. 1, 2014, pp. 212–222.

10. Chakravarty, A.: Four-Dimensional Fuel-Optimal Guidance in the Presence of Winds. *Journal of Guidance, Control, and Dynamics*, vol. 8, no. 1, 1985, pp. 16–22.

11. Chakravarty, A.; and Vagners, J.: 4-D Aircraft Flight Path Management in Real Time. *American Control Conference, 1983*, IEEE, 1983, pp. 794–795.

12. Burrows, J. W.: Fuel-optimal Aircraft Trajectories with Fixed Arrival Times. *Journal of Guidance, Control, and Dynamics*, vol. 6, no. 1, 1983, pp. 14–19.

13. Erzberger, H.; and Lee, H.: Constrained Optimum Trajectories with Specified Range. *Journal of Guidance, Control, and Dynamics*, vol. 3, no. 1, 1980, pp. 78–85.

14. Franco, A.; and Rivas, D.: Optimization of Multiphase Aircraft Trajectories Using Hybrid Optimal Control. *Journal of Guidance, Control, and Dynamics*, 2015, pp. 1–16. Doi:http://arc.aiaa.org/doi/pdf/10.2514/1.G000688.

15. Park, S. G.; and Clarke, J.-P.: Optimal Control Based Vertical Trajectory Determination for Continuous Descent Arrival Procedures. *Journal of Aircraft*, 2015. Doi:http://arc.aiaa.org/doi/abs/10.2514/1.C032967.

16. Khardi, S.: Aircraft Shortest and Fastest Continuous Descent Approach Development. *Journal of Aircraft*, vol. 49, no. 6, 2012, pp. 1931–1939.

17. Park, S. G.; and Clarke, J.: Fixed RTA Fuel Optimal Profile Descent Based on Analysis of Trajectory Performance Bound. *Digital Avionics Systems Conference (DASC), 2012 IEEE/AIAA 31st*, IEEE, 2012, pp. 3D3–1.

18. Windhorst, R.; Ardema, M.; and Kinney, D.: Fixed-Range Optimal Trajectories of Supersonic Aircraft by First-Order Expansions. *Journal of Guidance, Control, and Dynamics*, vol. 24, no. 4, 2001, pp. 700–709.

19. Andreeva-Mori, A.; Suzuki, S.; and Itoh, E.: Scheduling of Arrival Aircraft Based on Minimum Fuel Burn Descents. *ASEAN Eng J*, vol. 1, no. 1, 2011.

20. Roberson, B.; Root, R.; and Adam, D.: Fuel Conservation Strategies: Cost Index Explained. *Boeing Aero Quarterly*, vol. 2, no. 2007, 2007, pp. 26–45.

21. Rumler, W.; Günther, T.; Weißhaar, U.; and Fricke, H.: Flight Profile Variations due to the Spreading Practice of Cost Index Based Flight Planning. *4th International Conference on Research in Air Transportation, Budapest*, 2010.

22. Yosida, S.: Green's Theorem Method for a Control System with Outstanding Control. *Funkcialaj Ekvacioj*, vol. 16, 1973, pp. 255–263.

23. Korn, G. A.; and Korn, T. M.: *Mathematical Handbook for Scientists and Engineers: Definitions, Theorems, and Formulas for Reference and Review*. Courier Dover Publications, 2000.

24. Hale, F. J.: *Introduction to Aircraft Performance, Selection, and Design*. Wiley New York, 1984.

25. Pontryagin, L.: *Mathematical Theory of Optimal Processes*. Classics of Soviet Mathematics, Taylor & Francis, 1987. URL `http://books.google.com/books?id=kwzq0F4cBVAC`.

26. Bryson, Jr., A. E.; and Ho, Y.-C.: *Applied Optimal Control: Optimization, Estimation and Control*. CRC Press, 1975.

27. Slattery, R.; and Zhao, Y.: Trajectory Synthesis for Air Traffic Automation. *Journal of Guidance, Control and Dynamics*, vol. 20, no. 2, Mar. 1997, pp. 232–238.

28. Nuic, A.; Poinsot, C.; Iagaru, M.-G.; Gallo, E.; Navarro, F. A.; and Querejeta, C.: Advanced Aircraft Performance Modeling for ATM: Enhancements to the BADA Model. *Proceedings of the IEEE/AIAA 24th Digital Avionics Systems Conference*, Nov. 2005.

29. The MATLAB Software: *Version 7.7.0.471 (R2008b)*. The MathWorks Inc., Natick, 2008.

30. Benjamin, S. G.; Brown, J. M.; Brundage, K. J.; Schwartz, B.; Smirnova, T.; Smith, T. L.; Morone, L. L.; and Dimego, G.: The Operational RUC-2. Preprints. *Proceedings of the 16th Conference on Weather Analysis and Forecasting*, Amer. Meteor. Soc., 1998, pp. 249–252.

31. Bowe, A.; and Santiago, C.: An Approach for Balancing Delay and Fuel Burn in Separation Assurance Automation. *AIAA Aviation Technology, Integration, and Operations (ATIO) Conference*, 2012.

32. Robinson, J. E.; and Kamgarpour, M.: Benefits of Continuous Descent Operations in High-Density Terminal Airspace Under Scheduling Constraints. *Proceedings of the 10th AIAA Aviation Technology, Integration, and Operations Conference*, AIAA-2010-9115, Sept. 2010.

Appendix A

Direct Operating Cost as a Path Integral

The direct operating cost in Eq. (11) can be written as a path integral along the state trajectory [22]. First, rewrite the equations of motion in Eqs. (8) in a matrix form:

$$\begin{bmatrix} \dot{x} \\ \dot{V} \end{bmatrix} = \begin{bmatrix} (V+w) & 0 \\ -\overline{D} & 1 \end{bmatrix} \begin{bmatrix} 1 \\ \overline{T} \end{bmatrix}. \tag{A1}$$

Invert the two-by-two matrix on the right hand side to write the control $\overline{T}$ as a linear combination of $\dot{x}$ and $\dot{V}$ [22],

$$\overline{T} = \left(\frac{\overline{D}}{V+w} \right) \dot{x} + \dot{V}. \tag{A2}$$

Substituting Eq. (A2) into Eq. (11),

$$\overline{J} = \int_0^{t^f} \left\{ c_f \left[\left(\frac{\overline{D}}{V+w} \right) \dot{x} + \dot{V} \right] + \overline{r} \right\} dt.$$

Multiplying the last term by a factor of unity, $\dot{x}/(V+w)$,

$$\overline{J} = \int_0^{t^f} \left\{ c_f \left[\left(\frac{\overline{D}}{V+w} \right) \dot{x} + \dot{V} \right] + \frac{\overline{r}}{V+w} \dot{x} \right\} dt,$$

and changing the variables of integration,

$$\overline{J} = \int_\Gamma \left\{ \left[c_f \left(\frac{\overline{D}}{V+w} \right) + \frac{\overline{r}}{V+w} \right] dx + c_f \, dV \right\}. \tag{A3}$$

Here Γ stands for the trajectory, and dx and dV are related by the equations of motion and the control $\overline{T}$. Eq. (A3) expresses the cost function as a line integral of a differential form $P(x,V)dx + M(x,V)dV$, where

$$P(x,V) = \frac{c_f \overline{D} + \overline{r}}{V+w}, \text{ and } M(x,V) = c_f.$$

Appendix B

Optimal Control Strategy Connecting A State to the $[I = 0]$ Curve

The following lemma proves that the optimal control strategy for the problem considered in this work must use either $\overline{T}_{\min}$ or $\overline{T}_{\max}$ when connecting a state to the $[I = 0]$ curve.

Lemma 2 *A state trajectory that has no part in $I > 0$, has the final state on $[I = 0]$, and passes through a state $(x(t), V(t))$ in $I < 0$ at some instant t_*, with the control strategy $\overline{T}(t)$ strictly greater than $\overline{T}_{\min}$ in some neighborhood of t_*, is not optimal.*

Proof. Construct a new control strategy, denoted here by $\overline{T}_*(t)$, as follows. Replace $\overline{T}(t)$ by $\overline{T}_{\min}$ on the interval $[t_*, t_1]$, where t_1 is the earliest instant at which the newly obtained state trajectory, $(x_*(t), V_*(t))$, intersects either $(x(t), V(t))$ (Case (a)) or the curve $[I = 0]$ (Case (b)), whichever happens first (if the two cases coincide, the situation is treated as as Case (a)).

In Case (a), let $\overline{T}_*(t) = \overline{T}(t)$ for $t \geq t_1$, to obtain

$$\overline{T}_*(t) = \begin{cases} \overline{T}(t) & \text{for} \quad t < t_*, \\ \overline{T}_{\min} & \text{for} \quad t_* \leq t \leq t_1, \\ \overline{T}(t) & \text{for} \quad t_1 < t. \end{cases}$$

In Case (b), let $\overline{T}_*(t) = \overline{T}_{\text{mc}}(t)$ from $t = t_1$ until such earliest instant t_2 when $(x_*(t), V_*(t))$ intersects the $(x(t), V(t))$ (possibly at the final state). Assume this portion of arc on $[I = 0]$ is attainable. From $t = t_2$ on, let $\overline{T}_*(t) = \overline{T}(t)$. This yields

$$\overline{T}_*(t) = \begin{cases} \overline{T}(t) & \text{for} \quad t \leq t_*, \\ \overline{T}_{\min} & \text{for} \quad t_* \leq t \leq t_1, \\ \overline{T}_{\text{mc}}(t) & \text{for} \quad t_1 \leq t \leq t_2. \\ \overline{T}(t) & \text{for} \quad t_2 \leq t. \end{cases}$$

In both cases, $V_*(x)$ by construction satisfies both of the following conditions: $V_*(x) \leq V(x)$ for every x, and $V_*(x) < V(x)$ in some right-sided neighborhood of $x(t_*)$. By Lemma 1a at Section 4.2, $(x_*(t), V_*(t))$ outperforms $(x(t), V(t))$. This completes the proof.

Immediate consequences of Lemma 2, and of results analogous to it, are as follows:

(i) An optimal trajectory passing through a state (x, V) in $I < 0$ and later reaching $[I = 0]$ has in state (x, V) control $\overline{T}_{\min}$.

(ii) An optimal trajectory passing through a state (x, V) in $I > 0$ and later reaching $[I = 0]$ has in state (x, V) control $\overline{T}_{\max}$.

(iii) If an optimal trajectory passes through two states on $[I = 0]$, then the portion of the trajectory between these two states lies entirely on $[I = 0]$. (In other words, an optimal trajectory cannot leave $[I = 0]$ and then come back to $[I = 0]$.)

REPORT DOCUMENTATION PAGE

Form Approved
OMB No. 0704–0188

1. REPORT DATE *(DD-MM-YYYY)*	2. REPORT TYPE	3. DATES COVERED *(From - To)*
01-04-2015	Technical Memorandum	

4. TITLE AND SUBTITLE
Minimum-Cost Aircraft Descent Trajectories with a Constrained Altitude Profile

5a. CONTRACT NUMBER

5b. GRANT NUMBER

5c. PROGRAM ELEMENT NUMBER

6. AUTHOR(S)
Minghong G. Wu and Alexander V. Sadovsky

5d. PROJECT NUMBER

5e. TASK NUMBER

5f. WORK UNIT NUMBER

7. PERFORMING ORGANIZATION NAME(S) AND ADDRESS(ES)
NASA Ames Research Center
Moffett Field, California, 94035-1000

8. PERFORMING ORGANIZATION REPORT NUMBER
L–00000

9. SPONSORING/MONITORING AGENCY NAME(S) AND ADDRESS(ES)
National Aeronautics and Space Administration
Washington, DC 20546-0001

10. SPONSOR/MONITOR'S ACRONYM(S)
NASA

11. SPONSOR/MONITOR'S REPORT NUMBER(S)
NASA/TM–2015–218734

12. DISTRIBUTION/AVAILABILITY STATEMENT
Unclassified-Unlimited
Subject Category 00
Availability: NASA CASI (443) 757-5802

13. SUPPLEMENTARY NOTES
An electronic version can be found at http://ntrs.nasa.gov.

14. ABSTRACT
An analytical formula for solving the speed profile that accrues minimum cost during an aircraft descent with a constrained altitude profile is derived. The optimal speed profile first reaches a certain speed, called the minimum-cost speed, as quickly as possible using an appropriate extreme value of thrust. The speed profile then stays on the minimum-cost speed as long as possible, before switching to an extreme value of thrust for the rest of the descent. The formula is applied to an actual arrival route and its sensitivity to winds and airlines' business objectives is analyzed.

15. SUBJECT TERMS
EDA, fixed flight path angle descent, fuel burn

16. SECURITY CLASSIFICATION OF:			17. LIMITATION OF ABSTRACT	18. NUMBER OF PAGES	19a. NAME OF RESPONSIBLE PERSON
a. REPORT	b. ABSTRACT	c. THIS PAGE			STI Help Desk (email: help@sti.nasa.gov)
U	U	U	UU	19	19b. TELEPHONE NUMBER *(Include area code)*: (443) 757-5802